A computerized scheme for localization of vertebral bodies on body CT scans

Tatsuro Hayashi *[a], Huayue Chen [b], Kei Miyamoto [c], Xiangrong Zhou [a], Takeshi Hara [a], Ryujiro Yokoyama [d], Masayuki Kanematsu [d, e], Hiroaki Hoshi [f], Hiroshi Fujita [a]
[a] Department of Intelligent Image Information, Division of Regeneration and Advanced Medical Sciences, Graduate School of Medicine, Gifu University, 1-1 Yanagido, Gifu 501-1194, Japan;
[b] Department of Anatomy, Division of Disease Control, Graduate School of Medicine, Gifu University, 1-1 Yanagido, Gifu 501-1194, Japan;
[c] Department of Reconstructive Surgery for Spine, Bone, and Joint, Gifu University Graduate School of Medicine, 1-1 Yanagido, Gifu 501-1194, Japan;
[d] Radiology Services, Gifu University Graduate School of Medicine and University Hospital, 1-1 Yanagido, Gifu 501-1194, Japan;
[e] Department of Radiology, Gifu University Graduate School of Medicine and University Hospital, 1-1 Yanagido, Gifu 501-1194, Japan;
[f] Department of Radiology, Division of Tumor Control, Graduate School of Medicine, Gifu University, 1-1 Yanagido, Gifu 501-1194, Japan

ABSTRACT

The multidetector row computed tomography (MDCT) method has the potential to be used for quantitative analysis of osteoporosis with higher accuracy and precision than that provided by conventional two-dimensional methods. It is desirable to develop a computer-assisted scheme for analyzing vertebral geometry using body CT images. The aim of this study was to design a computerized scheme for the localization of vertebral bodies on body CT images. Our new scheme involves the following steps: (i) Re-formation of CT images on the basis of the center line of the spinal canal to visually remove the spinal curvature, (ii) use of information on the position of the ribs relative to the vertebral bodies, (iii) the construction of a simple model on the basis of the contour of the vertebral bodies on CT sections, and (iv) the localization of individual vertebral bodies by using a template matching technique. The proposed scheme was applied to 104 CT cases, and its performance was assessed using the Hausdorff distance. The average Hausdorff distance of T2–L5 was 4.3 mm when learning models with 100 samples were used. On the other hand, the average Hausdorff distance with 10 samples was 5.1 mm. The results of our assessments confirmed that the proposed scheme could provide the location of individual vertebral bodies. Therefore, the proposed scheme may be useful in designing a computer-based application that analyzes vertebral geometry on body CT images.

Keywords: Body CT images, Vertebral body, Localization, Template matching, Computerized scheme

1. INTRODUCTION

Osteoporosis has been estimated to affect more than 200 million individuals worldwide. One in three women and one in eight men are affected by osteoporosis [1]. Lateral spine radiography and dual-energy X-ray absorptiometry (DXA) are commonly used to determine the magnitude of osteoporosis and/or osteoporotic fractures. However, the accuracy and precision of these methods are limited because of their two-dimensional (2D) nature.

Recently, multidetector row computed tomography (MDCT) enabled high-resolution visualization of three-dimensional (3D) spine structures. The MDCT method has the potential to be used for the quantitative analysis of osteoporosis with higher accuracy and precision than that provided by conventional 2D methods. However, when thin-section CT is used to scan the whole body, a huge number of images—exceeding 1000 sections—are generated. Analysis of the spine using all these CT sections imposes a heavy burden on examiners. Therefore, it would be useful to develop a computer-assisted scheme to analyze vertebral geometry on body CT images.

Medical Imaging 2011: Image Processing, edited by Benoit M. Dawant, David R. Haynor,
Proc. of SPIE Vol. 7962, 796238 · © 2011 SPIE · CCC code: 1605-7422/11/$18 · doi: 10.1117/12.877511

Computer-based applications for analyzing the spine would benefit greatly from a computerized scheme for vertebral segmentation or identification on body CT images. To this end, several computerized schemes based on implicit anatomic knowledge [2, 3], four-dimensional curvature [4], surface-based registration [5], CT number thresholding and circularity [6], paradigm of mathematical morphology [7], the probabilistic model [8, 9], and the deformable model [10, 11] have been reported. However, due to the complex anatomy of both the normal and degenerated spine, spondylarthrotic and osteochondrotic deformations as well as calcifications of discoligamentous structures may be misinterpreted as "fusions" or "junctions" of the vertebrae. Therefore, designing a computerized scheme that can perform vertebral segmentation or identification accurately can be a challenging task.

Klinder et al. [12] presented a novel approach that involved curved planar re-formation of the spine and models that addressed the shape, gradient, and appearance. They were able to process arbitrary CT scans (head-neck, thoracic, lumbar, and whole spine images) as well as normal and pathologic spines. However, the success rates for identifying certain individual vertebrae were low. Ma et al. [13] also presented a sophisticated approach that is comparable to Klinder et al.'s approach. However, the average success rate for the identification of individual vertebrae was 73.1% when using a single vertebra. A state-of-the-art approach is needed to develop a robust scheme that can process arbitrary CT scans. However, some applications may not need to process such scans. For example, we analyzed body CT images to investigate the vertebral trabecular bone mineral density [14]. A computerized scheme that can process only body CT scans is sufficient for such a purpose.

It is thought that to design a sophisticated scheme for the localization of individual vertebral bodies, it would be helpful first to design a computer-assisted scheme to analyze vertebral geometry. Although extraction of intervertebral discs (or end plates) is one of the effective approaches, missing an intervertebral disc leads to failure in the localization of vertebral bodies. Pattern matching or a registration-based approach can also localize vertebral bodies without extracting intervertebral discs. However, variations in the individual's posture during CT scans or individual differences in spinal curvature may contribute to the performance deterioration of such an approach. In terms of implicit anatomic knowledge, ribs and thoracic vertebrae are contiguous bones. For that reason, we assume that the detection of individual ribs contributes to the scheme's improved performance for the localization of individual vertebral bodies.

In this paper, we present a computerized scheme for the localization of vertebral bodies on body CT images. Our new scheme was designed to have the following key steps: (i) Re-forming CT images on the basis of the center line of the spinal canal to visually remove the spinal curvature, (ii) using the information on the relative position between ribs and vertebral bodies, (iii) the construction of a simple model (reference pattern) on the basis of the contour of the vertebral bodies on CT sections, and (iv) the localization of individual vertebral bodies by using a template matching technique.

2. METHODS

2.1 Study sample

The CT images, which were obtained with a CT scanner (LightSpeed Ultra, GE Yokogawa Medical Systems Ltd., Tokyo, Japan), were scanned for the purpose of examining various organs and tissues, as is done in a metastasis check or follow-up. The scans included thoracic and lumbar vertebrae, and were scanned for each patient using standard settings (120 kV, auto mAs, 1.25-mm-thick slice, pitch = 0.59–0.82 mm). Slice intervals were modified to the same value as the pitch using sin*c* interpolation to keep each voxel in an isotropic size in 3D. The study sample consisted of 104 individuals (55 men and 49 women; mean age, 55.9 years). Those who had a normal variant at the vertebrae, as confirmed by radiologists or anatomic experts, were not included in this sample. This study was approved by the institutional review board of Gifu University.

2.2 Overview of the scheme

The proposed scheme is outlined in Fig. 1. It consists of the learning phase and the localization phase. The image re-formation technique, which is performed on the basis of the detection/extraction of bone parts, is applied in both phases. The localization of vertebral bodies is carried out using a template matching technique. The details of each stage of the scheme are described below.

2.3 Image re-formation

At the beginning of the image re-formation technique, bone extraction and detection of the center line of the spinal canal, the tips of the spinous processes, and the ribs (boundary with vertebrae) are attempted. Examples of these extractions and detections are shown in Fig. 2.

CT numbers with bone voxels are higher than those of other internal organs. CT number thresholding or the region-growing method is used to extract bone voxels [2]. Fig. 2a shows an example of the extraction of bone voxels.

We can observe the spinal canal as a cave inside the spine. For that reason, the centroid of the cave on the Jacoby line (an upper boundary slice with a false pelvis) is determined. After that, it is tracked in the craniocaudal direction [15].

Spinous processes can be observed as tips of bone behind the spinal canal. Therefore, these tips of bone are detected on axial sections excluding the tail sections from the Jacoby line. Detection of the center line of the spinal canal and tips of spinous processes in three axial sections (from top to bottom: T6, T11, and L3) are shown in Fig. 2b. In these sections, yellow and red circles denote centroids of the spinal canal and tips of spinous processes, respectively.

Ribs are contiguous bones with the spine. In our scheme, ribs are detected on the basis of their distance from the spinal canal. The detailed process is as follows:

1: Bone voxels within r mm of the center line of the spinal canal are extracted as standard voxels. Extraction examples in three axial sections are illustrated in Fig. 2b. In these sections, standard voxels and other bone voxels are indicated with green and blue, respectively.

2: The distance map from standard voxels is generated. The distance is calculated by the shortest path through the bone voxels.

3: The histogram of the distance map is generated, and its mode and a standard deviation are computed. While frequency values increase with increasing distance within the spine, they decrease with increasing distance at the ribs because they are thinner than the spine. Therefore, the following equations are defined for dividing three bone labels (*spine_label*, *boundary_label*, and *the_others_label*) using the distance map:

$$0 < spine\_label \le d_1, \tag{1}$$

$$d_1 < boundary\_label \le d_2, \tag{2}$$

$$d_2 < the\_others\_label, \tag{3}$$

$$d_1 = mode\_value + standard\_deviation \cdot b_1, \tag{4}$$

and

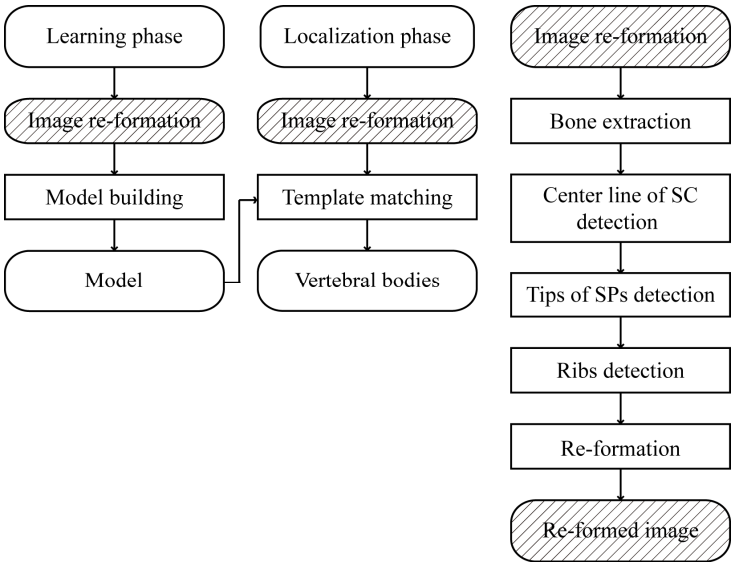

Fig.1 Process flow of the proposed scheme (spinal canal: SC, spinous processes: SPs).

$$d_2 = mode\_value + standard\_deviation \cdot b_2, \quad (5)$$

where d_1 and d_2 denote distance thresholds and b_1 and b_2 denote arbitrary variables. The histogram of the distance map and an example of the division into three bone labels are illustrated in Figs. 2c and 2d, respectively. In Fig. 2d, *spine_label*, *boundary_label*, and *the_others_label* are indicated in yellow, blue, and green, respectively. We can see the relation between distance map and bone labels in these figures.

4: Of the boundary labels, labels contiguous to both the *spine_label* and *the_others_label* are detected as *rib_candidate_labels*.

5: Of the *rib_candidate_labels*, 12 labels from the head are identified as the 1st–12th ribs. This identification is performed independently on the right and left sides. An example of 1st–12th ribs identification is demonstrated in Fig. 2e, in which the spine and the right and left ribs in each level are shown in yellow and the other colors, respectively.

To simplify the localization of vertebral bodies, CT images are re-formed on the basis of the spinal canal and spinous processes. The following three rules are applied to image re-formation.

1. Axial rotation is adjusted in each slice so that the line via the center line of the spinal canal and tips of the spinous processes (that is, the black dashed line shown in Fig. 3a) becomes the center in the sagittal direction.

2. Sagittal rotation is adjusted in each slice. Sagittal curvature at a target slice (an axial section) is defined as the angle between the centroids of the spinal canal on two axial sections (that is, SC_a and SC_b shown in Fig. 3b). Two axial sections are determined as those that are far from the *d* slices of the target.

3. Translation is carried out in each slice so that the center line of the spinal canal moves onto a straight line (Fig. 3c).

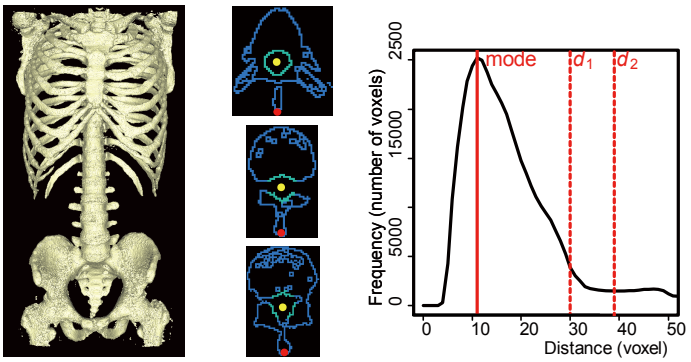

(a) (b) (c)

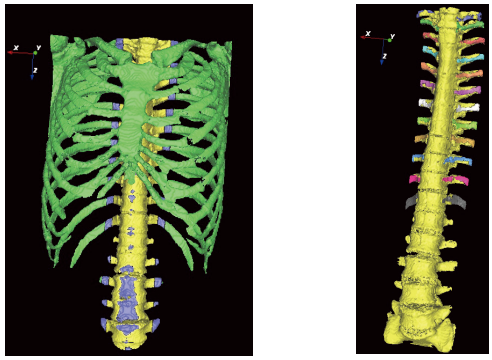

(d) (e)

Fig.2 Examples of bone parts detection/extraction in one case. (a) Surface view of bone voxels. (b) Three axial section views of bone voxels (top to bottom: T6, T11, and L3). Yellow and red circles denote centroids of the spinal canal and tips of spinous precesses, respectively, and standard voxels and other bone voxels are indicated in green and blue, respectively. (c) The histogram of the distance map. d_1 and d_2 denote distance thresholds for dividing bone labels. (d) Surface view of bone voxels divided into three labels (*spine_label*, *boundary_label*, and *the_others_label* are indicated in yellow, blue, and green, respectively). (e) Surface view of bone voxels identified right and left ribs in each level (spine and ribs in each level are shown in yellow and the other colors, respectively).

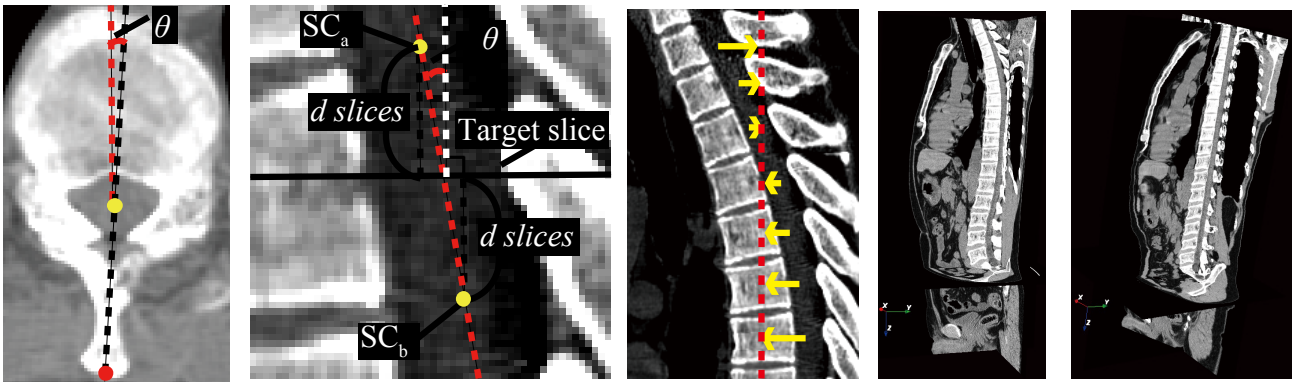

(a) (b) (c) (d) (e)

Fig.3 CT images re-formation based on the spinal canal and spinous processes. (a) An axial section view of the spine. Yellow and red circles denote centroid of the spinal canal and the tip of spinous processes, respectively, and an axial rotation of this section is defined as the angle between the black dashed line via centroid of the spinal canal and the tip of spinous processes and red dashed line that indicates vertical line. (b) A sagittal section view of the spine. SC_a and SC_b denote centroid of the spinal canal on two axial sections. Sagittal rotation at a target slice is defined as the angle between the red dashed line via SC_a and SC_b and the white dashed line that indicates vertical line. (c) A sagittal section view of the spine. The translation is performed so that the center line of the spinal canal moves onto the straight line (red dashed line). (d) Section view of CT images. We can see the spinal curvature. (e) Section view of re-formed images. We can see the spine without its rotation and curvature.

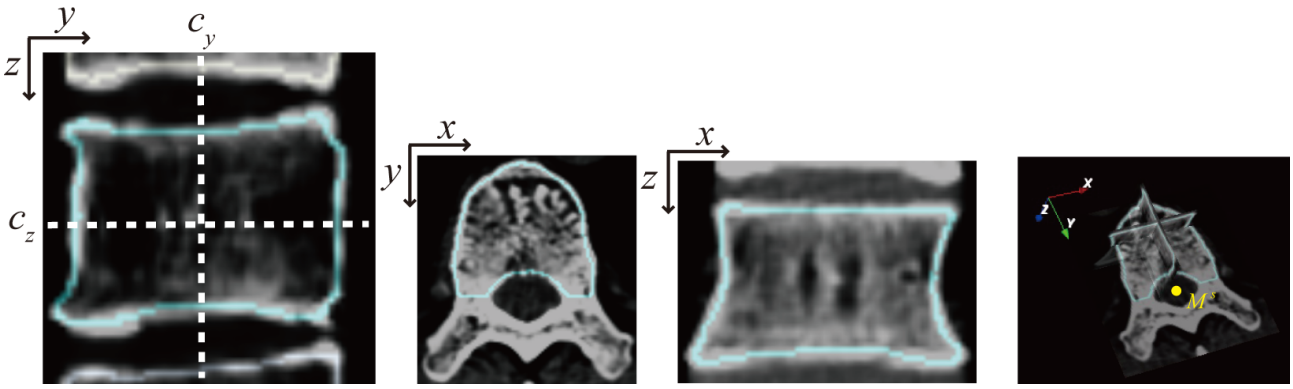

(a) (b) (c) (d)

Fig.4 Model building based on the contour tracking (Tracked contours are indicated in blue). (a) An example of the tracked contour on the sagittal section. c_y and c_z denote the center position in the tracked contour on this section. (b) An example of the tracked contour on the axial section at c_z. (c) An example of the tracked contour on the coronal section at c_y. (d) Examples of tracked contours on three sections.

Examples of CT images and re-formed CT images are demonstrated in Figs. 3d and 3e, respectively. We can see the spine in the reformed images without its rotation and curvature, as shown in Fig. 3e.

2.4 Learning phase

CT images are re-formed to the beginning of a learning phase using the above-mentioned process. After that, the contour models of each vertebral body are built on the re-formed images as follows:

1. Contours of vertebral bodies (T1–L5) are tracked on the sagittal central section (Fig. 4a).
2. Contours of the vertebral bodies are tracked on axial and coronal sections through the center of the vertebral bodies that were tracked by the preceding process (that is, the axial section at c_z and the coronal section at c_y, as shown in Fig. 4a). Examples of tracked contours on the axial and coronal sections are illustrated in Figs. 4b and 4c, respectively.
3. Tracked contours are registered as relative coordinates from the center point (one from the center line, M^s) of the spinal canal. M^s, which is the centroid of the spinal canal on the axial section at c_z, is defined as the standard coordinate of the model. Examples of tracked contours on three sections are shown in Fig. 4d.

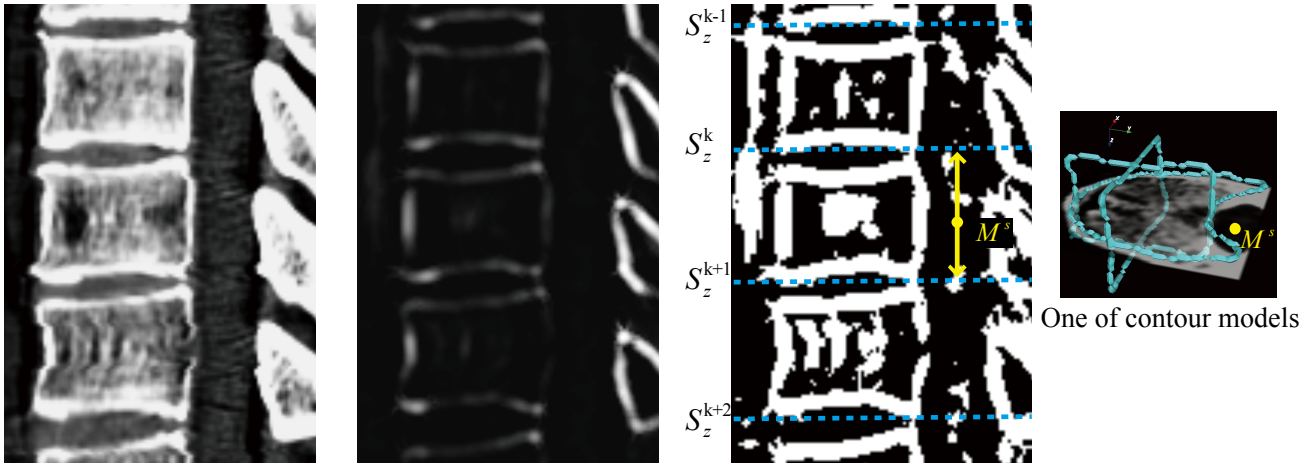

Fig.5 Localizations of vertebral bodies by using a template matching technique. (a) Sagittal central section on the re-formed images. (b) Images after top-hat operation. (c) Left: Images after binarized operation. Right: One of contour models indicates in blue. Blue voxels denote contours of the model.

2.5 Localization phase

CT images are re-formed to the beginning of a localization phase using the above-mentioned process. After that, the vertebral bodies are localized as follows:

1. The morphological top-hat operation is applied to the target (re-formed) images, and voxels with > 5 values are extracted as contour candidates of vertebral bodies. The target images, images after top-hat operation, and images after binarized operation are shown in Figs. 5a, 5b, and 5c (left side), respectively.

2. Ribs are utilized for the localization of thoracic vertebrae. First, the shortest paths that connect the ribs on both sides via bone voxels for the *k*th ribs $(k = 1,2,\cdots,12)$ are computed. After that, axial sections of one point, $S_z^k(k = 1,2,\cdots,12)$, nearest to the center line of the spinal canal for each path are detected. As for lumbar vertebrae, axial sections are predicted on the basis of the upper ribs.

$$S_z^k = S_z^{k-1} + \left(S_z^{k-1} - S_z^{k-2}\right)\ (k = 13,14,\cdots,18). \tag{6}$$

3. A template matching between the output of process 1 and models of vertebral bodies is performed to determine the precision between them. In the template matching, a rigid transformation is applied to the models, and the model whose precision indicates the highest value is determined to be the target vertebral body. The rigid transformation is applied according to the following restrictions:

I. Scaling, $s(0.9 \le s \le 1.1)$, is applied to the models.

II. Rotation, $r(-3.0° \le r \le 3.0°)$, is applied to the models.

III. Translation along the center line of the spinal canal is applied to the models. Ranges of translation are set for each vertebral body. For the *k*th thoracic vertebral bodies, the standard coordinate of models should meet the following requirement:

$$S_z^k \le M_z^s \le S_z^{k+1} \qquad (k = 1,2,\cdots,12), \tag{7}$$

and for the *k*th lumbar vertebral bodies, the standard coordinate of models should meet the following requirement:

$$S_z^{k+12} \le M_z^s \le S_z^{k+13} \qquad (k = 1,2,\cdots,5). \tag{8}$$

Translation of the model is illustrated in Fig. 5c. The percent of precision *P* of the template matching is calculated by the following equation:

$$P = \frac{P_A \cap P_B}{P_A}, \tag{9}$$

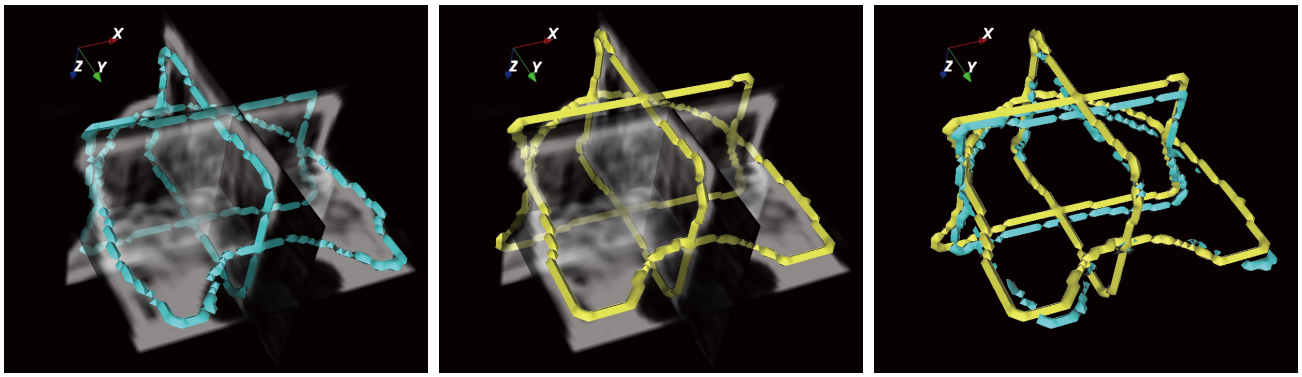

(a) (b) (c)

Fig.6 Examples of the measurement by using the Hausdorff distance. (a) Points of contours of vertebral bodies by manual (blue). (b) Points produced using the proposed scheme (yellow). (c) Overlaid image of two point sets. Hausdorff distance between two point sets is determined as the performance assessment.

where P_A denotes voxels making up the model and P_B denotes voxels extracted by the process 1.

2.6 Assessment

The Hausdorff distance [16], which is used to measure the boundary-based distance, is used to demonstrate the effect of our scheme. Given two finite point sets $A = \{a_1, a_2, \cdots, a_p\}$ and $B = \{b_1, b_2, \cdots, b_p\}$, the Hausdorff distance is defined as

$$H(A,B) = \max(h(A,B), h(B,A)), \tag{10}$$

where

$$h(A,B) = \max_{a \in A} \min_{b \in B} \|a - b\|, \tag{11}$$

and $\|\cdot\|$ is some underlying norm on the points of A and B. In this study, the points of the contour of vertebral bodies tracked on reformatted images (ground truth) and points produced using the proposed scheme were input as A and B, respectively, and the Euclidean norm was used as the underlying norm. Measurement of the Hausdorff distance is illustrated in Fig. 6.

3. RESULTS

To assess the performance of the proposed scheme, it was applied to 104 body CT cases. Learning models were built with 103 samples except for the target case, and parameters were set as r = 16 mm, d = 20 slices, b_1 = 3.0, and b_2 = 4.5 for this experiment. These parameters were decided by trial and error. The localization performance from T2 to L5 was assessed in this study because T1 was outside of the CT scans with some cases. Experimental results from two cases are illustrated in Fig. 7. The assessment result of the proposed scheme by use of the Hausdorff distance is shown in Fig. 8, in which we can see the Hausdorff distance (mean and standard deviation) with 104 cases in each vertebral level. The mean and standard deviations of the Hausdorff distance for the localization of vertebral bodies were 3.6–5.5 and 1.0–1.9 mm, respectively.

In addition, the following experiment was carried out to verify the effect of the learning models:

1. $k = \{10, 20, \cdots, 100\}$ samples were selected at random from 103 cases (except the target case).
2. Samples selected by process 1 were used to build the learning models.
3. Localizations of vertebral bodies were carried out using models built by process 2. After that, the Hausdorff distance between the localization result and the ground truth was measured.
4. Processes 1 – 3 were attempted 10 times, and the mean Hausdorff distance of their results was calculated.

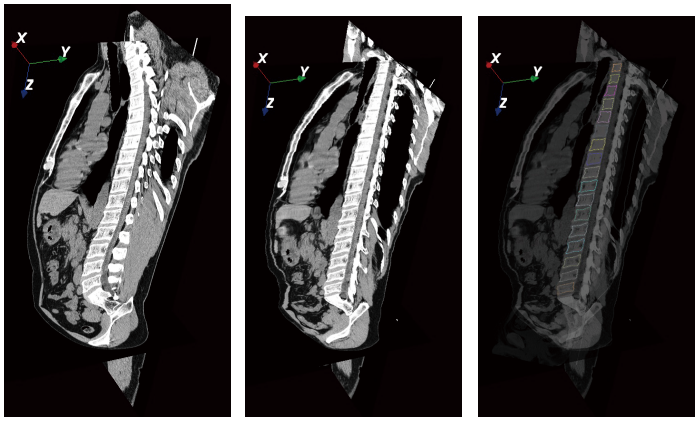

Fig.7 Experimental results from two cases. Left: Section view of CT images. Middle: Section view of the re-formed images. Right: Section view of the overlaid images between the re-formed images and points produced using the proposed scheme. Localization results of individual vertebral bodies are indicated in different colors.

The change in the mean Hausdorff distance according to the number of learning samples for the localization of vertebral bodies is shown in Fig. 9, which shows the mean Hausdorff distance at T3, T10, L1, L5, and the average of T2–L5. The average Hausdorff distance of T2–L5 from the learning models with 100 samples was 4.3 mm. On the other hand, the average Hausdorff distance with 10 samples was 5.1 mm. In terms of vertebral level, the Hausdorff distance with L3–L5 was larger than that of other vertebrae.

4. DISCUSSION

We designed a computerized scheme for the localization of vertebral bodies on body CT images. There have been similar studies, For example, Chwialkowski et al. [17] presented a computerized scheme for the localization and identification of the spinal anatomy on MR scans. However, their targets were limited to lumbar and lumbosacral vertebrae. Takahashi et al. [4] presented a computerized scheme for segmentation of vertebrae and measurement of bone mineral density and height on CT images. In their scheme, information on the position of the ribs was used to search the end plates. However, there was no quantitative assessment of the segmentation of vertebrae. Klinder et al. [12] presented a novel model-based approach for the segmentation of vertebrae on CT images. Ma et al. [13] presented a sophisticated approach based on edge detection. To process arbitrary CT images, they designed a computerized scheme that focused only on vertebrae. As a result, their scheme could process head-neck, thorax, lumbar, or whole-spine CT scans. However, the success rate in the identification of certain individual vertebrae was low. Experimental results for our study proved that our scheme could localize vertebral bodies at 3.6–5.5 mm of the Hausdorff distance on body CT images. Therefore, we believe that our scheme can be beneficial in designing a computer-assisted scheme for analyzing vertebral geometry on body CT images.

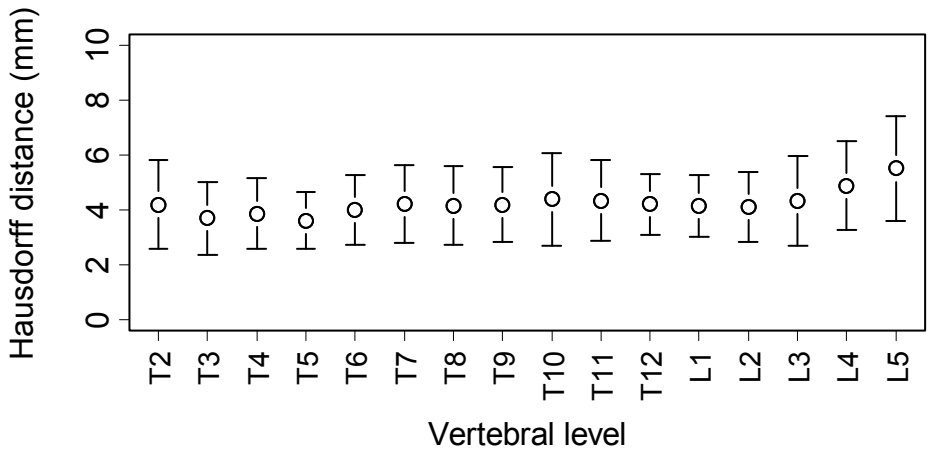

Fig.8 Performance assessment by the Hausdorff distance. The mean and standard deviation of the Hausdorff distance for individual vertebral bodies by 104 cases are shown in circle and error bar, respectively.

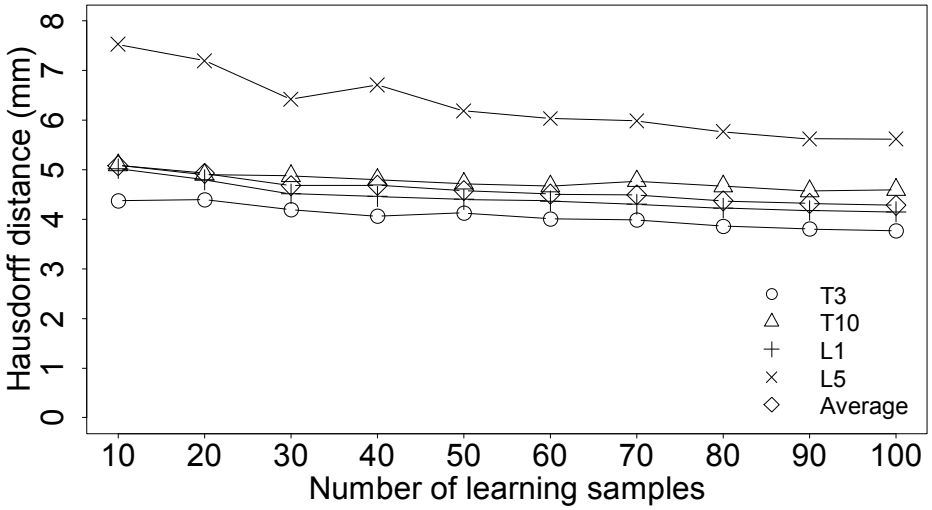

Fig.9 The change in the mean Hausdorff distance according to the number of learning samples for the localization of vertebral bodies. The mean Hausdorff distances at T3, T10, L1, L5, and the average of T2 – L5 are shown.

Our scheme was designed on the basis of information on the position of the ribs, contour models of vertebral bodies, and a template matching technique. The learning models were simple structures built using only three sections (axial, coronal, and sagittal). Even though just ten samples were utilized to build the learning models, our scheme could localize the vertebral bodies at 5.1 mm of the mean Hausdorff distance. However, the end plate of the neighboring vertebral body rather than the target vertebral body was detected in some cases, as shown in Fig. 10. As for the main causes of incorrect localization, the vertical edges of vertebral cortical bones were barely emphasized by the morphological top-hat operation. As a result, the precision of the template matching technique between the end plate of the target vertebral body and the neighboring vertebral body made almost no difference. It may be necessary to design an improved scheme that emphasizes vertebral cortical bones. On the whole, the Hausdorff distance with L3–L5 was larger than that of the other vertebrae. The thoracic vertebrae are near the ribs because of the contiguous bones, while the lumbar vertebrae (particularly the inferior vertebrae) are far from the ribs. For that reason, the effect of the information on the position of the ribs for the localization of vertebral bodies at L3–L5 would have been weak. To solve this problem, it may be necessary to design a scheme to detect costal processes.

Alignment of the spine, including cervical lordosis, thoracic kyphosis, lumbar lordosis, and sacral slope, contributes to maintaining its function. These spinal curves and slopes vary depending on the individual. In addition, scoliosis

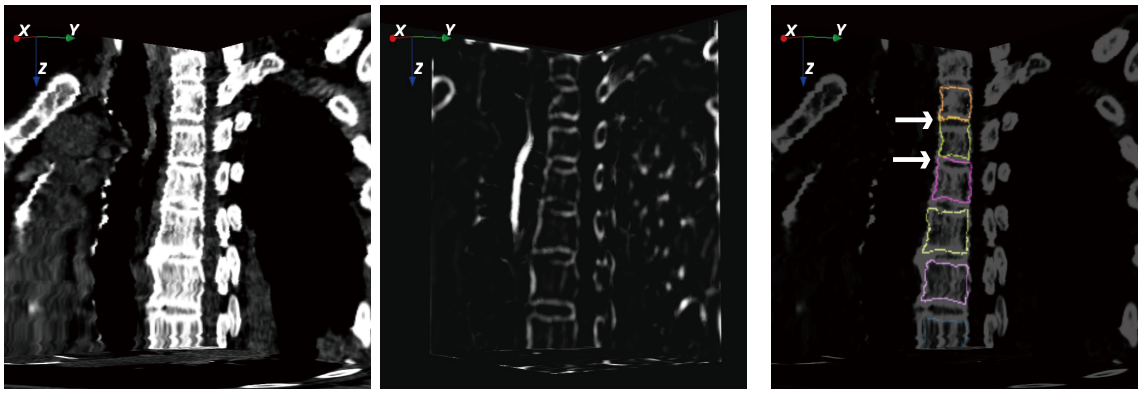

(a) (b) (c)

Fig.10 Examples of incorrect localization of vertebral bodies. (a) Section view of the re-formed images. (b) Section view of the images after top-hat operation. (c) Section view of the overlaid images between the re-formed images and points produced using the proposed scheme. Localization results of individual vertebral bodies are indicated in different colors. White arrows show the positions of incorrect localization of vertebral bodies.

patients experience lateral curvature and axial rotation of the spine. For that reason, in our efforts to localize vertebral bodies, it would be useful to design a scheme for normalization of the spinal alignment. Some automated curved planar reformation (CPR) algorithms have been presented [11, 12, 18]. Hanaoka et al. [11] presented a CPR algorithm based on detection of intervertebral discs. Their approach was advantageous in that it could perform not only spinal straightening but also vertebral size adjustment. However, their approach required an algorithm that was detailed enough to manage the complicated spinal alignment. In this study, we designed an algorithm for image re-formation based on the center line of the spinal canal and the tips of the spinous processes. Although our algorithm could not adjust for vertebral size, it could re-form images without detecting intervertebral discs.

The proposed scheme does have some limitations. Our scheme cannot process images that do not include ribs, such as head-neck or lumbar CT scans. Furthermore, when detecting individual ribs, the scheme operates on the basis of implicit anatomic knowledge that ribs and thoracic vertebrae are contiguous bones. However, as is the case for some body CT scans, part of T1 (specifically the connection between T1 and the first rib) was outside of the images. In such cases, our scheme did not detect the first rib. For that reason, it may be necessary to perform a check of the scan ranges before using the proposed scheme.

As a follow-up to this study, we plan to design a computerized scheme for measuring vertebral geometry, and to investigate age- and gender-dependent changes in vertebral geometry using large-scale body CT images.

5. CONCLUSION

A computerized scheme for the localization of vertebral bodies on body CT images was designed. The proposed scheme made use of information on the position of individual ribs, an image re-formation technique, and a template matching technique. On the basis of the results of our assessments, we confirmed that the proposed scheme could provide the location of individual vertebral bodies. Therefore, the proposed scheme may be useful in designing a computer-based application that analyzes vertebral geometry on body CT images.

ACKNOWLEDGEMENTS

The authors thank members of the Fujita Laboratory for their valuable discussions, and grateful to Gifu University Hospital staffs for preparing the CT cases, especially for Mr. T. Miyoshi and Mr. Y. Inoue. This research was supported in part by a research grant of Grant-in-Aid for Young Scientists B (21700462) froms Japan Society for the Promotion of Science (JSPS), in part by a research grant from Japan Osteoporosis Foundation, and in part by a research grant of Grant-in-Aid for Scientific Research on Priority Areas (21103004) of the Ministry of Education, Culture, Sports, Science, and Technology, Japan.

REFERENCES

[1] NE Lane, "Epidemiology, etiology, and diagnosis of osteoporosis," *Am J Obstet Gynecol*, 194 (2 Suppl): S3-11 (2006)

[2] X Zhou, T Hayashi, M Han, H Chen, T Hara, H Fujita, R Yokoyama, M Kanematsu, and H Hoshi, "Automated segmentation and recognition of the bone structure in non-contrast torso CT images using implicit anatomical knowledge," *Proc of SPIE Medical Imaging 2009, Image Processing*, 7259: 72593S-1-72593S-4 (2009)

[3] S Furuhashi, K Abe, M Takahashi, T Aizawa, T Shizukuishi, M Sakaguchi, T Maebayashi, I Tanaka, M Narata, and Y Sasaki, "A computer-assisted system for diagnostic workstations: Automated bone labeling for CT images," *J Digit Imaging*, 22: 689-695 (2009)

[4] E Takahashi, S Saita, Y Kawata, N Niki, M Itoh, H Nishitani, and N Moriyama, "Computer aided diagnosis for osteoporosis using multi-slice CT images," *Proc of SPIE Medical Imaging 2010, Computer-Aided Diagnosis*, 7624: 76243Q-1-76243Q-8 (2010)

[5] JL Herring, BM Dawant, "Automatic lumbar vertebral identification using surface-based registration," *J Biomed Inform*, 34: 74-84 (2001)

[6] S Nishihara, H Fujita, T Iida, A Takigawa, T Hara, and X Zhou, "Evaluation of osteoporosis in X-ray CT examination: A preliminary study for an automatic recognition algorithm for the central part of a vertebral body using abdominal X-ray CT images," *Comput Med Imaging Graph*, 29: 259-266 (2005)

[7] B Naegel, "Using mathematical morphology for the anatomical labeling of vertebrae from 3D CT-scan images," *Comput Med Imaging Graph*, 31: 141-156 (2007)

[8] JJ Corso, RS Alomari, and V Chaudhary, "Lumbar disc localization and labeling with a probabilistic model on both pixel and object features," *Med Image Comput Comput Assist Interv*, 11: 202-210 (2008)

[9] S Schmidt, J Kappes, M Bergtholdt, V Pekar, S Dries, D Bystrov, and C Schnörr, "Spine detection and labeling using a parts-based graphical model," *Inf Process Med Imaging*, 20: 122-133 (2007)

[10] Y Kim, D Kim, "A fully automatic vertebra segmentation method using 3D deformable fences," *Comput Med Imaging Graph*, 33: 343-352 (2009)

[11] S Hanaoka, Y Nomura, M Nemoto, Y Masutani, E Maeda, T Yoshikawa, N Hayashi, N Yoshioka, and K Ohtomo, "Automated segmentation method for spinal column based on a dual elliptic column model and its application for virtual spinal straightening," *J Comput Assist Tomogr*, 34: 156-162 (2010)

[12] T Klinder, J Ostermann, M Ehm, A Franz, R Kneser, and C Lorenz, "Automated model-based vertebra detection, identification, and segmentation in CT images," *Med Image Anal*, 13: 471-482 (2009)

[13] J Ma, L Lu, Y Zhan, X Zhou, M Salganicoff, and A Krishnan, "Hierarchical segmentation and identification of thoracic vertebra using learning-based edge detection and coarse-to-fine deformable model," *Med Image Comput Comput Assist Interv*, 13: 19-27 (2010)

[14] T Hayashi, H Chen, K Miyamoto, X Zhou, T Hara, R Yokoyama, M Kanematsu, H Hoshi, and H Fujita, "Analysis of bone mineral density distribution at trabecular bones in thoracic and lumbar vertebrae using X-ray CT images," *J Bone Miner Metab*, [Epub ahead of print]

[15] T Hayashi, X Zhou, H Chen, T Hara, K Miyamoto, T Kobayashi, R Yokoyama, M Kanematsu, H Hoshi, and H Fujita, "Automated extraction method for the center line of spinal canal and its application to the spinal curvature quantification in torso X-ray CT images," *Proc. of SPIE Medical Imaging 2010, Image Processing*, 7623: 76233F-1-76233F-4 (2010)

[16] DP Huttenlocher, GA Klanderman, and WJ Rucklidge, "Comparing images using the Hausdorff distance," *IEEE Trans on Pattern Analysis and Machine Intelligence*, 15: 850-863 (1993)

[17] MP Chwialkowski, PE Shile, D Pfeifer, RW Parkey, and RM Peshock, "Automated localization and identification of lower spinal anatomy in magnetic resonance images," *Comput Biomed Res*, 24: 99-117 (1991)

[18] T Vrtovec, B Likar, and F Pernus, "Automated curved planar reformation of 3D spine images," *Phys Med Biol*, 50: 4527-4540 (2005)